All-Optical Radiation Reaction at 10^{21} W/cm^2

M. Vranic,[1,*] J. L. Martins,[1] J. Vieira,[1] R. A. Fonseca,[1,2] and L. O. Silva[1,†]
[1]*GoLP/Instituto de Plasmas e Fusão Nuclear, Instituto Superior Técnico, Universidade de Lisboa, 1049-001 Lisbon, Portugal*
[2]*DCTI/ISCTE–Instituto Universitário de Lisboa, 1649-026 Lisboa, Portugal*
(Received 19 June 2013; published 22 September 2014)

Using full-scale 3D particle-in-cell simulations we show that the radiation reaction dominated regime can be reached in an all-optical configuration through the collision of a ∼1 GeV laser wakefield accelerated electron bunch with a counterpropagating laser pulse. In this configuration the radiation reaction significantly reduces the energy of the particle bunch, thus providing clear experimental signatures for the process with currently available lasers. We also show that the transition between the classical and quantum radiation reaction could be investigated in the same configuration with laser intensities of 10^{23} W/cm^2.

DOI: 10.1103/PhysRevLett.113.134801 PACS numbers: 41.60.−m, 52.38.Kd, 52.65.Rr

Radiation reaction is the change of momentum of a charged particle while it radiates. This apparently simple problem has many subtleties and it remains a long-standing fundamental question yet to be fully understood [1,2]. The Lorentz-Abraham-Dirac (LAD) equation was an attempt to self-consistently account for the radiation reaction in the classical regime [3]. However, this equation contains unphysical runaway solutions and violates the causality principle, which gave rise to various alternative models to account for this effect [2,4–7]. In particular, the model proposed by Landau and Lifshitz (LL) [4] contains all the physical solutions of the LAD equation [8], is free of the problems aforementioned [8,9], and is therefore a strong candidate to describe the classical radiation reaction.

There is also a strong debate about the threshold at which the quantum effects prevail [5,6,10]. Former experimental studies observed pair production in a 53 GeV electron beam interaction with a 10^{18} W/cm^2 intensity laser, but their parameters were such that the average energy loss per electron was only on the order of a few percent due to the low photon emission rate. Once emitted, a single photon could carry tens of GeV in energy, with high probability of decaying into an e^+e^- pair [11,12]. This is the so-called "QED dominated regime." Here, we are interested in the radiation reaction dominated regime, where electrons give a small fraction of their energy to a single photon, but lose a notable amount of energy due to repeated photon emission. Many synchrotrons operate in this regime, so they have to reaccelerate the electrons to compensate for the energy lost to radiation.

Additional experimental configurations to explore the radiation reaction could enable us to study various aspects of this process in detail. Some experimental schemes with lasers towards this direction have recently been proposed [13,14], but a configuration where the radiation reaction dominated regime would have clear signatures remains to be identified and thoroughly tested. In this Letter, we identify a radiation reaction dominated regime using state-of-the-art lasers with intensities $\sim 10^{21}$ W/cm^2. Using three-dimensional full-scale *ab initio* particle-in-cell simulations, we explore an all-optical scheme based on head-on scattering a laser pulse off a laser wakefield accelerated (LWFA) GeV electron bunch. Electron bunches with 1.5 GeV energy and 100 pC charge have already been obtained experimentally in 1 cm long plasmas [15–17] in LWFA. Also, hard photons (a few hundreds of keV) were experimentally produced from a LWFA-accelerated electron beam interacting head-on with a laser pulse [18], which clearly indicates that this configuration is feasible. It is the purpose of this work to explore the classical radiation reaction effects for currently available laser and plasma parameters, and to identify signatures of this process. We find that the head-on collision between a LWFA generated electron bunch with energy 0.5–1.5 GeV, and a counterpropagating scattering laser pulse of intensity 10^{20}–10^{22} W/cm^2 (Fig. 1) leads to significant electron beam energy loss and energy-spread reduction that can be

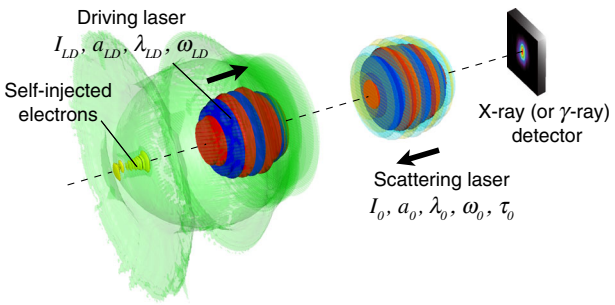

FIG. 1 (color online). All-optical radiation reaction configuration. A moderate intensity laser is used to generate the laser wakefield where the electrons are self-injected and accelerated. A counterpropagating ultrahigh intensity laser pulse collides head-on with the energetic electron bunch in vacuum after it leaves the plasma (cf. Supplemental Material, Movie 3 [19]).

easily detected in an experiment. The interaction is accompanied by hard x-ray emission. Effects such as the ponderomotive push away from the laser and relativistic mass shift are intrinsically included in our simulations and they would not hinder the observation of the radiation reaction in this configuration.

We start by analytically estimating how much energy the electrons lose during the interaction with the scattering laser pulse. For the sake of completeness, we examine the total radiated power (averaged over the solid angle) for a single electron undergoing Compton scattering in a plane electromagnetic wave [20] given by

$$P = -\frac{d(\gamma mc^2)}{dt} = c\sigma_C \gamma^2 (1 - \beta\cos\theta)^2 U_{PH} \qquad (1)$$

where σ_C is the Compton cross section (for the case of ultrarelativistic electrons, the Compton scattering cross section converges to the Thompson cross section $\sigma_C \approx \sigma_T = 8\pi r_0^2/3$), $r_0 = e^2/mc^2$ is the classical electron radius, e is the elementary charge, m is the electron mass, γ is the electron Lorentz factor, θ is the angle between the $\mathbf{k}$ vector of the counterpropagating electromagnetic wave and $\boldsymbol{\beta}$, the electron velocity normalized to c, and $U_{PH} = (E^2 + B^2)/8\pi$ is the energy density of the electromagnetic field. Equation (1) is valid for $\gamma\hbar\omega_0 \ll mc^2$ (ω_0 is the frequency of the electromagnetic wave), i.e., when in its rest frame the electron still undergoes the classical Thompson scattering. For an ultrarelativistic electron $|\boldsymbol{\beta}| \approx 1$, and Eq. (1) becomes

$$\frac{d\gamma}{dt} = -\frac{e^2\omega_0^2}{3mc^3}(1 - \cos\theta)^2 a_0^2 \gamma^2, \qquad (2)$$

where $a_0 = eA/mc^2$ is the normalized vector potential. In a plane wave with constant amplitude, Eq. (2) can be integrated to give $\gamma(t) = \gamma_0/(1 + \alpha t\gamma_0)$, where $\alpha = (e^2\omega_0^2/3mc^3)(1 - \cos\theta)^2 a_0^2$. Assuming the laser pulse is a plane wave with a temporal envelope $a_0(t)$, integration of Eq. (2) yields an estimate for the final electron energy after interacting with the scattering laser

$$\gamma_f = \frac{\gamma_0}{1 + k\gamma_0}, \qquad k = (1 - \cos\theta)^2 \frac{\eta}{3}\frac{e^2\omega_0^2}{mc^3} a_0^2 \tau_0, \qquad (3)$$

where γ_0 and γ_f are the initial and the final relativistic factor of the electron, τ_0 is the scattering laser pulse duration at FWHM in the laser fields, and a_0 is the peak normalized vector potential of the scattering laser. The crossing time between the laser and the electrons is $\approx\tau_0/2$. The factor $\eta \approx 0.4$ accounts for the different temporal profiles where, for instance, $\eta = 0.375$ for an envelope $a_0(t) = a_0 \sin^2(t\pi/2\tau_0)$, and $\eta = 0.392$ for the polynomial envelope we have used in the simulations (described later with other simulation parameters). The coefficient k depends only on the scattering laser, and can be written in a more convenient way as $k = 3.2 \times 10^{-5} I_0[10^{22}\ \mathrm{W/cm^2}]\tau_0[\mathrm{fs}](1 - \cos\theta)^2$, where I_0 is the scattering laser peak intensity. We can now relate the properties of the electron bunch with those of the plasma when a laser drives a LWFA [21]. The estimated output electron energy from a LWFA stage in the blowout regime is determined by $\gamma_0 = (2/3)(\omega_{\mathrm{LD}}/\omega_p)^2 a_{\mathrm{LD}}$, where ω_{LD} and a_{LD} are the frequency and the normalized vector potential of the laser driver, and $\omega_p = (4\pi n_e e^2/m)^{1/2}$ is the electron plasma frequency of the background plasma (n_e is the electron density). In a typical matched LWFA, the laser frequency ω_L takes values between $10\,\omega_p$ and $100\,\omega_p$. For a head-on collision, where $1 - \cos\theta \approx 2$, Eq. (3) shows that an electron beam looses 50% of the energy in the interaction with the scattering laser when $1 \simeq k\gamma_0 = 0.073 \times I_0[10^{22}\ \mathrm{W/cm^2}]\tau_0[10\ \mathrm{fs}]\sqrt{I_{\mathrm{LD}}[10^{22}\ \mathrm{W/cm^2}]}(\omega_{\mathrm{LD}}/\omega_p)^2$, which can be easily achieved (I_{LD} is the intensity of the driver laser).

Equation (3) also shows that the electron energy spread decreases during Compton scattering in this configuration, since faster electrons radiate a larger percentage of their energy than the less energetic ones. For a quasimonoenergetic electron beam the relative energy spread decreases at the same rate as the mean energy viz.

$$\frac{\delta\gamma_f}{\gamma_f} = \frac{1}{1 + k\gamma_0}\frac{\delta\gamma_0}{\gamma_0}. \qquad (4)$$

During the interaction with the scattering laser, the electron energy is converted into radiation. For relativistic electrons, the radiation is confined within a narrow angle that scales with $1/\gamma$ around the propagation direction. In our setup, the counterpropagating laser is linearly polarized in the x_3 direction, and propagates in the negative x_1 direction. The electrons wiggle in the laser polarization plane, and the maximum angle of the electron momentum with respect to the initial propagation direction is $p_3/p_1 \approx a_0/\gamma$. Then, the maximum angle for the radiation of a single electron from LWFA with $\gamma \simeq \gamma_0$ is given by $\theta_{\mathrm{rad}} = (3a_0/2a_{\mathrm{LD}})(\omega_p/\omega_{\mathrm{LD}})^2$.

The total number of backscattered photons during the interaction with the laser can be estimated according to $N_\gamma = N_e N_{\mathrm{col}}$, where N_{col} is the number of single photon-electron collisions per electron, and N_e is the number of electrons in the beam. The collision number can be obtained using the Compton cross section and the Poynting flux in the average electron rest frame [20]

$$N_{\mathrm{col}} = \frac{e^2 a_0^2 \omega_0}{8c\hbar}\tau_0 = 1.72 \times 10^{-3} a_0^2 \tau_0[\mathrm{fs}]\left(\frac{1\ \mu\mathrm{m}}{\lambda_0}\right), \qquad (5)$$

where λ_0 is the wavelength of the scattering laser. Equation (5) does not depend on the electron initial energy, but only on the photon density (laser intensity). Taking the

number of self-injected electrons in a matched LWFA, given by $N_e \simeq (1/30)(2\sqrt{a_{\rm LD}})^3(1/k_p r_0)$, where $k_p = \omega_p/c$ is the plasma wave number, we can then estimate the total number of single-scattering photons. This yields approximately $N_\gamma \simeq 1.497\times10^{12} I_0[10^{22}\,{\rm W/cm^2}]\lambda_0[\mu{\rm m}]\tau_0[10\,{\rm fs}]\times I_{\rm LD}^{3/4}[10^{22}\,{\rm W/cm^2}]\lambda_{\rm LD}^{3/2}[\mu{\rm m}]\lambda_p[\mu{\rm m}]$, where $\lambda_{\rm LD}$ is the wavelength of the driver.

Ideally, the goal would be to observe radiation reaction signatures in the radiated spectrum. However, this may be impossible due to several reasons. First, for a head-on collision of an electron and an electromagnetic wave with $a_0 \gg 1$, the photons are radiated in the nonlinear regime, where many harmonics appear. The fundamental frequency on-axis (first harmonic) here is given by $\omega_R \simeq 4\omega_0\gamma^2/\alpha$, where $\alpha = 1 + a_0^2/2$ for linear and $\alpha = 1 + a_0^2$ for circular laser polarization. Classically, this can be seen as a double Doppler shift of the laser photon due to the parallel component of the electron motion [22]. In QED, α comes from the electron relativistic mass shift [23,24]. Second, in a realistic laser pulse, electrons feel a different intensity over time, so the fundamental frequency also varies with time. This means that all the harmonics shift their positions in the frequency spectra. Note that N_γ estimates the number of photons in the first harmonic from the whole interaction with the laser pulse, but this part of the signal on the detector might be indistinguishable from the other harmonics. The lowest expected fundamental frequency is on the order of $\omega_R \simeq (16/9)(\omega_{\rm LD}/\omega_p)^4 a_{\rm LD}^2\omega_0/(1 + a_0^2/2)$, and for high a_0 we can expect more radiation at higher harmonics. For the GeV-class electron bunches with 30 fs laser pulses with $I_0 = 10^{21}$ W/cm^2, the lowest energy photons could be on the order of 44 keV, and $N_\gamma \simeq 10^{11}$. Third, the main effect of the radiation reaction is the slowdown of the colliding electrons, which in turn smears out the possible radiation signatures even more. In fact, as shown by Eqs. (1)–(3), in the aforementioned case the electron bunch energy decreases by more than 40%—this gives a clear and reliable signature to measure in laboratory conditions.

We now explore this configuration resorting to 3D full-scale particle-in-cell (PIC) simulations, over a wide range of parameters encompassing current and near future laser technology. In OSIRIS [25], a set of computational particles is moved under the action of electromagnetic field: this is done by first depositing the current density on a spatial grid, then solving Maxwell's equations on the same grid and computing the force accelerating each particle by interpolation of the field values on the position of the particle. As a fully relativistic PIC code, OSIRIS incorporates the relativistic mass shift, but does not include binary collisions or effects such as pair production. To include the classical radiation reaction, we have replaced the standard Lorentz force (LF) in the particle pusher with the LL equation [26]. Benchmarks shown in Supplemental Material [19] illustrate the effects of including LL over LF, and confirm that the effects explored in this Letter can only be attributed to the radiation reaction. By simulating Gaussian laser pulses in three dimensions, we include all the ponderomotive effects that might lead to electron beam breakup. We define the transverse spot size as $1/e$ in the fields, and the longitudinal laser envelope rises as $10\tau^3 - 15\tau^4 + 6\tau^5$, where $\tau = \sqrt{2}t/\tau_0$ and τ_0 is the pulse duration at FWHM. Laser parameters for different simulations are summarized in Table I, while the plasma and technical simulation parameters are summarized in the Supplemental Material, Table 1 [19]. Lasers a, b, c were used in the LWFA stage to accelerate electrons, which, after leaving the plasma, interacted with intense scattering lasers A–E in vacuum.

The scattering laser pulses spot sizes (10 μm) are much wider than the transverse width of the LWFA electron bunches (on the order of 2 microns) to guarantee that all the electrons in the bunch interact with an approximately uniform transverse laser profile (cf. Supplemental Material, Movie 3 [19]). Thus Eqs. (1)–(3) can be employed to estimate the electron energy loss in the interaction. Large energy losses (40% for 1 GeV electrons colliding with a 10^{21} W/cm^2 laser) can be easily measured in an experiment, even if the electron bunch is not quasimonoenergetic (see Fig. 2 and the Supplemental Material, Fig. 1 [19]). Excellent agreement between analytical and numerical results is obtained, as shown in Fig. 3. The χ_e parameter in Fig. 3 represents the ratio between the maximal laser electric field amplitude in the electron rest frame and the critical Schwinger field [27], and the curve corresponding to $\chi_e = 1$ marks the theoretical transition

TABLE I. Laser parameters for the parameter scan. LWFA with lasers a, b, and c and plasma slabs with density of the order 10^{18} cm^{-3} are simulated in matched conditions for the blowout regime [21], leading to acceleration of 0.5, 1, and 1.5 GeV electron bunches, respectively. As they leave the plasma, electron bunches are scattered by counterpropagating lasers A, B, C, D, or E. All the lasers have wavelengths of 1 μm.

Laser driver			a	b	c
$a_{\rm LD}$			4	8	9
Spot - $W_{\rm LD}$ [μm]			13	18	22
Duration - $\tau_{\rm LD}$ [fs]			42.4	60.0	73.3
Power - $P_{\rm LD}$ [PW]			0.044	0.349	0.658
Energy - $E_{\rm LD}$ [J]			1.855	21	48.2
Intensity - $I_{\rm LD}$ [10^{20} W/cm^2]			0.22	0.88	1.1
$\omega_{\rm LD}/\omega_p$			20	20	23
Scattering laser	A	B	C	D	E
a_0	8.55	17.1	27.0	54.0	85.5
W_0 [μm]	10	10	10	10	10
τ_0 [fs]	26.5	26.5	26.5	26.5	26.5
P_0 [PW]	0.123	0.491	1.23	4.91	12.3
E_0 [J]	4	16.4	40.8	164	410
I_0 [10^{20} W/cm^2]	1	4	10	40	100

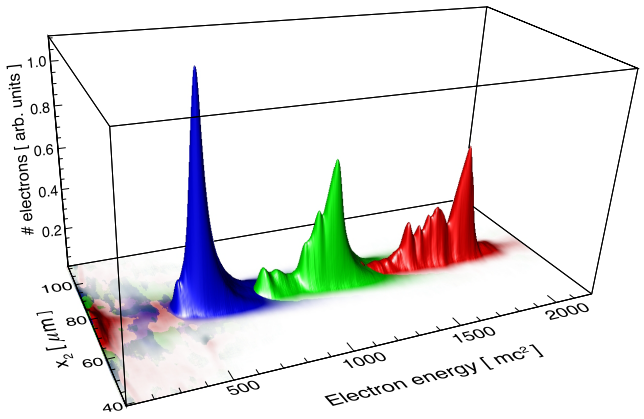

FIG. 2 (color online). LWFA electron beam profile initially, and after interaction with two different lasers. The initial beam profile given in red, and after interacting with a 10^{21} W/cm^2 laser (in green) or after interacting with a 4×10^{21} W/cm^2 (in blue). The peak positions are in agreement with the theoretical predictions of Eq. (3).

between the classical radiation reaction dominated regime and the QED regime [28]. Figure 3 shows that the near-future laser technology with intensities above 10^{22} W/cm^2, in combination with multi-GeV electron bunches, will approach the QED regime while having ~80% average electron energy loss—this will give an insight to physics experimentally unexplored to date.

The electron beam emittance and divergence can change slightly during the laser interaction [30], but not enough to jeopardize the beam detection. Emittance growth due to beam electron-plasma ion interaction is negligible, as well as the electron-electron collisions within the beam [31,32]. Lasers with nonideal transverse intensity profiles may change the output energy of LWFA electrons [33], but this also would not affect the observation of radiation reaction signatures as long as the beam spectra is characterized (e.g., in terms of the peak energy of the beam).

To evaluate a single electron radiation output, we can numerically integrate test electron trajectory in the laser field with and without accounting for the radiation reaction in otherwise identical conditions (see Fig 4). A postprocessing diagnostic JRAD [34] uses the phase-space trajectory of the electrons to calculate the total energy received in each pixel of a virtual detector located 4 cm in front of the interaction region. The detector receives in total 493 MeV when the radiation reaction is not included in the electron motion [Fig. 4(a)], and 311 MeV if the radiation reaction is accounted for [Fig. 4(b)]. The total energy loss of the test electron due to the radiation reaction is 315 MeV [Fig. 4(d)]. This means that the purely classical calculations, which ignore the radiation reaction, overestimate the total emitted radiation in this scenario and lead to results that violate energy conservation laws. As expected, the energy lost by the electron when accounting for the radiation reaction is fully consistent with the photon energy captured on the detector. Figure 4(e) shows the radiated energy of the 1 GeV electron beam interacting with the laser of intensity $I = 10^{21}$ W/cm^2 (combination *b-C* from Table I). The beam from the PIC simulation is represented by a 1% random sample and the detector captures over 99% of the energy lost by these electrons.

Analytical estimates, full-scale 3D PIC simulations including the radiation reaction and a postprocessing radiation diagnostic, all consistently predict the same electron energy loss, which is measurable in present-day laboratory conditions, and thus provide a direct signature for radiation reaction and a path to explore the classical to quantum radiation reaction transition.

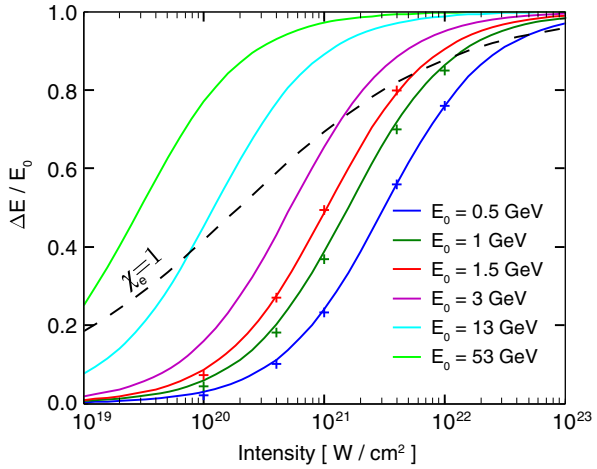

FIG. 3 (color online). Electron beam energy loss. Parameter scan based on *ab initio* full scale PIC simulations for different experimental conditions that correspond to 0.5, 1, and 1.5 GeV—class LWFA electron beams, coupled with a scattering laser with intensity in the range 10^{20}–10^{22} W/cm^2. Curves represent the theoretical prediction of Eq. (3), and each cross represents one simulation result. For reference, the theoretical curves for higher energy electron beams from Ref. [29] are also given; the dashed black line corresponds to the value $\chi_e = 1$.

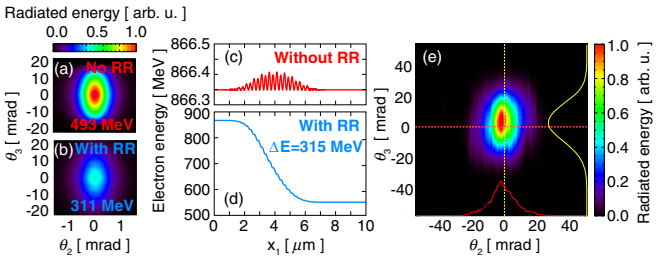

FIG. 4 (color online). Radiation. The radiated energy captured on a virtual detector (a) without and (b) with radiation reaction; evolution of the corresponding electron energy vs longitudinal position, without (c) and with (d) the radiation reaction; (e) radiated energy from an OSIRIS simulation of a 1 GeV electron bunch interacting with laser *C*. Note the horizontal scale change, so a single electron contribution is a thin vertical line here.

We thank Professor S. Bulanov and Dr. T. Grismayer for fruitful discussions. This work is supported by the European Research Council (ERC-2010-AdG Grant 267841) and FCT (Portugal) Grants PTDC/FIS/111720/2009, SFRH/BD/62137/2009, and SFRH/BD/39523/2007. Simulations were performed at Jugene (Germany) under a PRACE Grant, IST cluster (Lisbon, Portugal), and Jaguar (Oak Ridge, USA) under an INCITE Grant.

*marija.vranic@ist.utl.pt
†luis.silva@ist.utl.pt

[1] F. Rohrlich, Phys. Lett. A **283**, 276 (2001).
[2] F. V. Hartemann and N. C. Luhmann, Phys. Rev. Lett. **74**, 1107 (1995).
[3] P. A. M. Dirac, Proc. R. Soc. A **167**, 148 (1938).
[4] L. D. Landau and E. M. Lifshitz, *The Classical Theory of Fields* (Butterworth Heinemann, Washington, DC, 1975).
[5] A. R. Bell and J. G. Kirk, Phys. Rev. Lett. **101**, 200403 (2008).
[6] I. V. Sokolov, N. M. Naumova, J. A. Nees, G. A. Mourou, and V. P. Yanovsky, Phys. Plasmas **16**, 093115 (2009).
[7] G. Ford and R. O'Connell, Phys. Lett. A **157**, 217 (1991).
[8] H. Spohn, Europhys. Lett. **50**, 287 (2000).
[9] F. Rohrlich, Phys. Rev. E **77**, 046609 (2008).
[10] Y. Hadad, L. Labun, J. Rafelski, N. Elkina, C. Klier, and H. Ruhl, Phys. Rev. D **82**, 096012 (2010).
[11] C. Bula, K. T. McDonald, E. J. Prebys, C. Bamber, S. Boege, T. Kotseroglou, A. C. Melissinos, D. D. Meyerhofer, W. Ragg, D. L. Burke, R. C. Field, G. Horton-Smith, A. C. Odian, J. E. Spencer, D. Walz, S. C. Berridge, W. M. Bugg, K. Shmakov, and A. W. Weidemann, Phys. Rev. Lett. **76**, 3116 (1996).
[12] D. L. Burke, R. C. Field, G. Horton-Smith, J. E. Spencer, D. Walz, S. C. Berridge, W. M. Bugg, K. Shmakov, A. W. Weidemann, C. Bula, K. T. McDonald, E. J. Prebys, C. Bamber, S. J. Boege, T. Koffas, T. Kotseroglou, A. C. Melissinos, D. D. Meyerhofer, D. A. Reis, and W. Ragg, Phys. Rev. Lett. **79**, 1626 (1997).
[13] A. Di Piazza, K. Z. Hatsagortsyan, and C. H. Keitel, Phys. Rev. Lett. **102**, 254802 (2009).
[14] A. G. R. Thomas, C. P. Ridgers, S. S. Bulanov, B. J. Griffin, and S. P. D. Mangles, Phys. Rev. X **2**, 041004 (2012).
[15] W. P. Leemans, B. Nagler, A. J. Gonsalves, C. Toth, K. Nakamura, C. G. R. Geddes, E. Esarey, C. B. Schroeder, and S. M. Hooker, Nat. Phys. **2**, 696 (2006).
[16] S. Kneip, S. R. Nagel, S. F. Martins, S. P. D. Mangles, C. Bellei, O. Chekhlov, R. J. Clarke, N. Delerue, E. J. Divall, G. Doucas, K. Ertel, F. Fiuza, R. Fonseca, P. Foster, S. J. Hawkes, C. J. Hooker, K. Krushelnick, W. B. Mori, C. A. J. Palmer, K. Ta Phuoc, P. P. Rajeev, J. Schreiber, M. J. V. Streeter, D. Urner, J. Vieira, L. O. Silva, and Z. Najmudin, Phys. Rev. Lett. **103**, 035002 (2009).
[17] D. H. Froula, C. E. Clayton, T. Döppner, K. A. Marsh, C. P. J. Barty, L. Divol, R. A. Fonseca, S. H. Glenzer, C. Joshi, W. Lu, S. F. Martins, P. Michel, W. B. Mori, J. P. Palastro, B. B. Pollock, A. Pak, J. E. Ralph, J. S. Ross, C. W. Siders, L. O. Silva, and T. Wang, Phys. Rev. Lett. **103**, 215006 (2009).
[18] K. Ta Phuoc, S. Corde, C. Thaury, V. Malka, A. Tafzi, J. P. Goddet, R. C. Shah, S. Sebban, and A. Rousse, Nat. Photonics **6**, 308 (2012).
[19] See Supplemental Material at http://link.aps.org/supplemental/10.1103/PhysRevLett.113.134801 for benchmarks and a full description of the simulations, additional physics, and media.
[20] G. B. Rybicki and A. P. Lightman, *Radiative Processes in Astrophysics* (John Wiley & Sons, New York, 1979).
[21] W. Lu, M. Tzoufras, C. Joshi, F. S. Tsung, W. B. Mori, J. Vieira, R. A. Fonseca, and L. O. Silva, Phys. Rev. ST Accel. Beams **10**, 061301 (2007).
[22] E. Esarey, S. K. Ride, and P. Sprangle, Phys. Rev. E **48**, 3003 (1993).
[23] A. I. Nikishov and V. I. Ritus, Sov. Phys. JETP **19**, 529 (1964).
[24] J. Koga, T. Z. Esirkepov, and S. V. Bulanov, Phys. Plasmas **12**, 093106 (2005).
[25] R. A. Fonseca, L. O. Silva, F. S. Tsung, V. K. Decyk, W. Lu, C. Ren, W. B. Mori, S. Deng, S. Lee, T. Katsouleas, and J. C. Adam, *Lecture Notes on Computer Science* (Springer, Berlin, Heidelberg, 2002), Vol. 2331, p. 342.
[26] M. Vranic, J. L. Martins, and L. O. Silva, Bull. Am. Phys. Soc. **54**, 71 (2009), http://meetings.aps.org/Meeting/DPP09/Session/CP8.71.
[27] J. Schwinger, Phys. Rev. **82**, 664 (1951).
[28] S. Bulanov, T. Esirkepov, Y. Hayashi, M. Kando, H. Kiriyama, J. Koga, K. Kondo, H. Kotaki, A. Pirozhkov, S. Bulanov, A. Zhidkov, P. Chen, D. Neely, Y. Kato, N. Narozhny, and G. Korn, Nucl. Instrum. Methods Phys. Res., Sect. A **660**, 31 (2011).
[29] S. F. Martins, R. A. Fonseca, W. Lu, W. B. Mori, and L. O. Silva, Nat. Phys. **6**, 311 (2010).
[30] E. Esarey, Nucl. Instrum. Methods Phys. Res., Sect. A **455**, 7 (2000).
[31] C. B. Schroeder, E. Esarey, C. G. R. Geddes, C. Benedetti, and W. P. Leemans, Phys. Rev. ST Accel. Beams **13**, 101301 (2010).
[32] T. Katsouleas, Am. J. Phys. **60**, 568 (1992).
[33] J. Vieira, S. F. Martins, F. Fiuza, C. K. Huang, W. B. Mori, S. P. D. Mangles, S. Kneip, S. Nagel, Z. Najmudin, and L. O. Silva, Plasma Phys. Controlled Fusion **54**, 055010 (2012).
[34] J. L. Martins, S. F. Martins, R. A. Fonseca, and L. O. Silva, Proc. SPIE Int. Soc. Opt. Eng. **7359**, 73590V (2009).